Environmental Modelling and Software 125 (2020) 104616

Contents lists available at ScienceDirect

Environmental Modelling and Software

journal homepage: http://www.elsevier.com/locate/envsoft

# QUIC-fire: A fast-running simulation tool for prescribed fire planning

R.R. Linn [a,*], S.L. Goodrick [b], S. Brambilla [a], M.J. Brown [a], R.S. Middleton [a], J.J. O'Brien [b], J.K. Hiers [c]

[a] Los Alamos National Laboratory, Los Alamos, NM, 87545, USA
[b] USDA Forest Service Center for Forest Disturbance Science, Athens, GA, 30602, USA
[c] Tall Timbers Research Station, Tallahassee, FL, 32312, USA

ARTICLE INFO

*Keywords:*
Fire behavior model
Fire-atmospheric feedbacks
Cellular automata
Prescribed fire model

ABSTRACT

Coupled fire-atmospheric modeling tools are increasingly used to understand the complex and dynamic behavior of wildland fires. Multiple research tools linking combustion to fluid flow use Navier-Stokes numerical solutions coupled to a thermodynamic model to understand fire-atmospheric feedbacks, but these computational fluid dynamics approaches require high-performance computing resources. We present a new simulation tool called QUIC-Fire to rapidly solve these feedbacks by coupling the mature 3-D rapid wind solver QUIC-URB to a physics-based cellular automata fire spread model Fire-CA. QUIC-Fire uses 3-D fuels inputs similar to the CFD model FIRETEC, allowing this tool to simulate effects of fuel structure on local winds and fire behavior. Results comparing fire behavior metrics to the computational fluid dynamic model FIRETEC show strong agreement. QUIC-Fire is the first tool intended to provide an opportunity for prescribed fire planners to compare, evaluate, and design burn plans, including complex ignition patterns and coupled fire-atmospheric feedbacks.

## 1. Introduction

Wildland fire behavior and subsequent fire effects are largely driven by complex heterogenous and dynamic fire-atmospheric feedbacks (Hilton et al., 2015; Linn et al., 2013). Understanding the complex interactions of ignition pattern, heterogeneous vegetation, and dynamic fire environmental conditions are critical to accurately predicting fire behavior (Hoffman et al., 2018) and subsequent fire effects (O'Brien et al., 2018). Many fire behavior models have been developed to predict fire spread, energy release, and fire effects using a variety of approaches (Sullivan, 2009a, 2009b), but ultimately all wildland fire models must balance representing the complexity of fire-fuel-atmospheric feedbacks and the speed of predictions (Hilton et al., 2018). In addition, firefighter safety and rapid assessments of fire spread have dominated the objectives for much of the modeling to date, leading to adoption of tools producing rapid outputs as a preference over models that capture complex wildland fire dynamics.

This bias for speed over accuracy is particularly problematic for prescribed fire practitioners who must account for complex ignition patterns and dynamic environmental conditions (i.e., wind and moisture) to plan and execute burning treatments. Intentional ignitions are used to manage 5 million hectares annually in the US (Melvin, 2015) with many millions more burned globally (Bond and Keeley, 2005; Guyette et al., 2017; Ichoku et al., 2008). Planning and development of legal prescriptions for prescribed fire practices to meet objectives depends on anticipating the fire's response to variation in fuels and weather conditions (Chiodi et al., 2018; O'Brien et al., 2018; Wade et al., 1989). One complication to the prediction of prescribed fire behavior compared to wildfire scenarios is the significant influence of the rates and patterns of ignition on fire behavior. Also, the interaction between the fire environment and practitioner-designed ignition practices depends on landscape-scale mean fuel and weather conditions as well as their localized spatial and temporal variability (Canfield et al., 2014; Furman, 2018). In managed fire regimes, surface fire behavior is further complicated by three-dimensional turbulent flows within the canopy (Parsons et al., 2011; Pimont et al., 2011) and by surrounding edge effects such as those produced by roads or adjacent previously burned blocks (Linn et al., 2012). In this case, fuel structure influences wind flow through the canopy in the vicinity of the surface fires, affecting air entrainment among firelines and draw between fires. To cope with such complexity and ultimately the spread patterns and intensity potential of fires, managers are forced to rely exclusively on experience or rules of thumb (Cruz and Alexander, 2019) as the simplified models of forward fire spread available to plan fire activities do not account for these kinds

* Corresponding author. Earth and Earth Sciences Division, Los Alamos National Laboratory, Los Alamos, NM, 87545, USA.
*E-mail address:* rrl@lanl.gov (R.R. Linn).

https://doi.org/10.1016/j.envsoft.2019.104616
Received 2 August 2019; Received in revised form 23 December 2019; Accepted 26 December 2019
Available online 28 December 2019
1364-8152/

of critical processes (Mell et al., 2018).

There are a variety of models that have been developed to generate rapid wildfire behavior predictions, such as the fire spread model of Rothermel (1972) and its derivatives, including Behave (Andrews, 1986), FARSITE (Finney, 1998), and Prometheus (Tymstra et al., 2010). These models are either empirically derived from algebraic regressions of fire behavior observations, or semi-empirical solutions employing simplified physical bases for their algebraic functional forms with the addition of calibration constants calculated from fire behavior observations (Sullivan, 2009a, 2009b). The algebraic functional forms of these models describe the spread of wildfires as functions of mean local ambient conditions such as wind speed, fuel conditions and topographic slope. They do not, however, resolve the individual processes that produced the fire behavior. Such approaches extrapolate the single fireline behavior to complex patterns of firelines, ignoring the effect of the fire and atmosphere interactions, thus misrepresenting the spreading behavior and the fire intensity. In fact, multiple ignitions commonly used in prescribed fires or wildfire suppression tactics violate several key assumptions of most simplified wildfire spread models, such as steady state fire spread, non-interacting firelines, (Yedinak et al., 2018), and homogeneity of fuels (Hiers et al., 2009). Improving the effectiveness of prescribed fire management requires new modeling tools designed to capture the complex dynamics of multiple firelines, heterogeneous fuels, and variable environmental conditions (Hoffman et al., 2018; O'Brien et al., 2018).

To represent the influences of the dynamic interaction between fire, fuel, and atmosphere, fire behavior models have been linked to computational fluid dynamics (CFD) models that characterize the movement of the atmosphere (Linn et al., 2002; Mell et al., 2007). Current models that explicitly represent some aspect of fire behavior and associated atmospheric response to fires fall into two categories: 1) empirical fire spread models coupled to an atmospheric fluid dynamics model (e.g., WRF-Fire, Coen et al., 2013; WRF-SFire, Mandel et al., 2011; CAWFE, Coen, 2013) and 2) process-based fire models coupled to an atmospheric fluid dynamics model (e.g., WFDS, Mell et al., 2007; FIRETEC, Linn et al., 2002; FIRESTAR, Morvan et al., 2007). The challenge for the use of the former class of fire-atmosphere models for prescribed fire is that they are designed to run at horizontal resolutions >20 m where the representations of the fire and atmospheric perturbations are smoothed to larger scales in order to be consistent with the underpinning empirical basis of the fire models. These scales are then too coarse to simulate prescribed-fire dynamics or the fuel heterogeneity that drives prescribed-fire behavior, which are often smaller than 10 m. The challenge for the process-based coupled fire-atmosphere models is the computational demands of these models, which typically exceed the time or computer resources for practical use in planning prescribed fires.

Achtemeier (2013) used a cellular automata (CA)-based approach to model the movement of fire based on a set of rules attached to observed or theoretical phenomenology. Because CA models attempt to represent some of the local phenomenology of fires, which is dominated by local winds, it is possible to couple them to flow models to capture some of the two-way feedbacks between fires and the atmosphere. Achtemeier et al. (2012) coupled their CA model to a simplified wind model and produced promising results using only a limited set of rules based on the expert opinion of the developer. Such 2D fire spread can then be coupled to potential flow to rapidly predict fire spread (Hilton et al., 2018).

While the model of Achtemeier (2013) used a simple depth-averaged wind flow to model fire spread through a simplified localized spot-driven model, its ruleset was not directly tied to physical processes, which has led to limited adoption outside of its use within the Daysmoke model (Achtemeier et al., 2012). Additionally, fuel representation relied on 2D models of forest type with a rule-based influence of fuelbed height. While 2D representations are common and can simplify predictions (e.g. WRF S-fire (Hilton et al., 2018)), such simplifications limit potentially important fire-atmospheric interactions driven by 3D fuel variation (i.e., locally increased surface flows in stem spaces downwind of a canopy gap) in surface fire regimes (Parsons et al., 2011; Pimont et al., 2011). For realistic representation of fire behavior that drives fire effects in a prescribed fire setting, 3D time-resolved fire behavior must be coupled to more accurate representations of fuels (O'Brien et al., 2018). This is also critically important to understanding prescribed fire behavior which results from complex ignition patterns (Furman, 2018) as the response of fires to these ignition patterns depends on the local vertical and horizontal vegetation structure. The ability of a simplified model to rapidly and accurately represent fire-atmospheric feedbacks enabling representation of the interaction between multiple ignitions and 3D fuel structure would represent a crucial advancement.

Here, we describe a recently developed wildland fire modeling tool, QUIC-Fire, that uses a CA coupled fire-atmospheric modeling approach that builds on the approach by Achtemeier (2013) but applies physical process-based rules to achieve a more generalized fire spread model onto 3D fuel data. In the following sections model formulation, results of preliminary simulation results, lessons learned concerning the impacts of fire-atmosphere coupling, and a discussion of a path forward for this model are described.

## 2. Methods

### 2.1. QUIC-fire model description

QUIC-Fire is a wildland fire simulation tool designed to capture the coupled fire-atmosphere interactions that are essential for simulating prescribed fire without extreme computational demands. Its design allows for wider-spread use and ensemble calculations to cover, for instance, a range of possible weather or fuel conditions. Since we developed QUIC-Fire as a prescribed fire planning tool, it was purposefully designed to be able to represent the fire-atmosphere feedbacks that determine the behavior of prescribed fires as well as the influences of heterogeneous vegetation. This was accomplished by exploiting the capabilities of the QUIC-URB wind field solver (Pardyjak and Brown, 2003; Singh et al., 2008) coupled with a new CA-based fire spread model, referred to here as FIRE-CA. QUIC-URB is a fast-running wind field solver that was originally designed for computing flow fields around buildings in urban settings (Pardyjak and Brown, 2003). It combines mass conservation constraints with observation-based wind field phenomenology algorithms to quickly compute 3D flow fields that include the influence of both structure-driven drag and now, the dynamic buoyancy sources of wildland fires. The coupling between the extended QUIC-URB wind field solver and FIRE-CA was executed by passing a 3D vegetation and fire-influenced wind field associated turbulence intensity from QUIC-URB to drive FIRE-CA. FIRE-CA then feeds back the spatially resolved and evolving three-dimensional vegetation and heat release distributions to QUIC-URB.

### 2.2. Extension of QUIC-URB for wildland fire application

The presence of the fire alters the wind fields in two ways: through the buoyancy-driven flows and through its effects on the vegetation and resulting impacts on aerodynamic drag. In order to extend QUIC-URB for wildland fire scenarios, a representation of the strong buoyancy-induced flows was implemented. Part of the heat produced by the flames warms up the surrounding atmosphere, generating a buoyantly driven vertical movement of heated air. In turn, the displacement of the heated air draws in adjacent air to fill the vacated volume, producing a convergence zone. Ultimately, the resulting flow pattern influences the fire spread (Achtemeier et al., 2012). As the hot air travels upwards in an isolated plume, it mixes with fresh air and the volume that it influences increases with height while its upward velocity decreases. With sustained heat release, the rising parcels of air form a plume that increases in diameter with height and can lean downwind depending on local wind speed. To capture these phenomena, the plume trajectory and lateral expansion are parameterized with the Briggs theory (Davidson,

1989). With the Briggs theory, the plume radius and centerline updraft are recalculated at each point on the trajectory. For this approach, we initially assumed that there is non-zero local horizontal wind speed and thus as hot air rises it is also translating some horizontal distance, $x$, from the spot of plume origination. The centerline updraft ($w_c$) is a function of the heat released by the fire and the horizontal downwind distance from the point of origin (Davidson, 1989):

$$w_c = \frac{1}{\beta}\sqrt{\frac{2}{3}\frac{F_B}{w_s(z+z_{vert})}}$$

Here, $\beta$ is an empirical constant, $z_{vert}$ is an offset for a virtual plume origin, and $F_B$ is a buoyancy term (in $m^4\ s^{-3}$). $z_{vert}$ is related to cell size since it compensates for the fact that the plume is starting with an area that is the same as the horizontal area for the cell,

$$z\_vert = \frac{\sqrt{(A_{cell}/\pi)}}{\beta}$$

$F_B$ is defined by:

$$F_B = \frac{g}{T_a}\left(\frac{E}{\rho_a c_{p_a}}\right)$$

where $g$ is the acceleration due to gravity, $T_a$, $\rho_a$, and $c_{p_a}$ are the ambient air temperature, density and specific heat of the undisturbed air, and $E$ is the heat released by the fire in any given computational cell into the atmosphere (in Watts). Computationally, plumes are initiated from each QUIC-URB cell where heat is generated. Plume radii at the plumes' origin are computed from the horizontal area, $A_{cell}$, of the computational cell. The plumes develop over time under the influence of their own buoyancy and surrounding winds, which are influenced by the presence of other plumes as well. Plumes also influence each other. For instance, for two perfectly vertical nearby plumes, their trajectories will bend toward one another. In particular, the plume with the smaller buoyancy will bend more toward the one with higher buoyancy. This phenomenon requires $O(n^2)$ calculations, where $n$ is the number of plumes. Hence, tracking three-dimensional plumes emanating from every heated cell is very computationally intensive. However, the plumes of hot gases rising from nearby locations eventually merge. Thus, in order to streamline computations, two plumes are merged when their trajectories are closer than the sum of their radii, that is, when the plumes start to overlap. The updraft of the merged plume is calculated based on Lai and Lee (2012) and the merged plume radius recalculated to guarantee mass conservation. A Gaussian similarity profile is used to describe the radial updraft decay. This updraft is superimposed onto the QUIC-URB solution while the resulting horizontal flow is established by imposing mass consistency.

As fire consumes fuels, drag is reduced and the horizontal wind speed increases. QUIC-URB incorporates a Cionco-type correlation to parameterize the vegetation drag (Cionco, 1965; Nelson et al., 2009); here we applied a novel solution to the drag dynamics by linearly interpolating wind speed between the calculated Cionco profile (representing the unburnt canopy) and the unimpeded flow (representing a fully burnt canopy). In particular, the wind speed is a function of the reduction in vegetation due to fire consumption. For example, in the absence of fire-induced flows, the wind profile in the absence of vegetation is a log-law profile as is typical of the atmosphere (Sutton, 1953), but in the presence of the vegetation canopy the wind profile within the canopy is slower than would be predicted by the log-law (Fig. 1). As the canopy burns, the wind speed value moves along the black line in Fig. 1. The drag impact on local wind in each cell that initially has fuel in it is adjusted as the fire progresses, depending on the local fuel consumption at a specific time.

In the context of a spreading fire that is consuming vegetation, this modification in QUIC-URB successfully captured the higher wind speeds in areas where fuels were consumed. The procedure also enables the wind field to reflect some of the influences of the spatial distribution of fuel treatments and fuel heterogeneity.

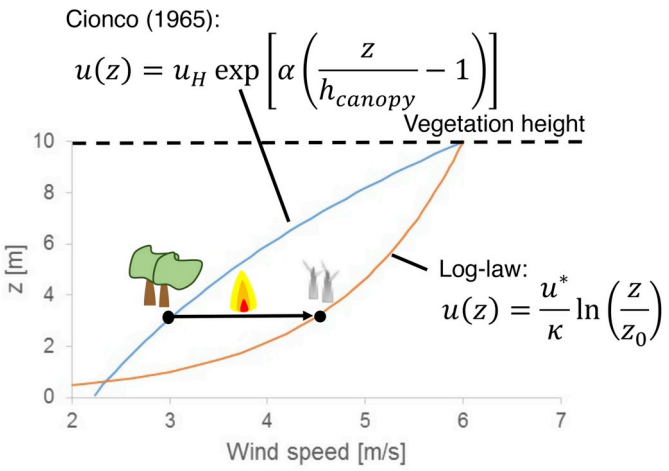


**Fig. 1.** The Cionco profile (Cionco, 1965) was used to parameterize the vegetation drag while the log-law profile would be used if no vegetation was present. As the fuel burns, the wind speed is increased linearly between the two extremes. For instance, at a height of 3.5 m, the wind speed will increase from 3 m $s^{-1}$ for the unscathed canopy to 4.7 m $s^{-1}$ after all the fuel is consumed by the fire.

### 2.3. FIRE-CA

FIRE-CA is built on a conceptual model that leverages the work of Achtemeier et al. (2012) and Achtemeier (2013) where the energy transfer from one location to another is accomplished through a cellular automata (CA) approach. In FIRE-CA, energy packets (EPs) are moved from one location to another based on local wind environments. EPs either evaporate moisture, start new fires, intensify existing fires, or transfer their energy to the atmosphere based on the fuel conditions in their destination cells. Each EP represents a fixed amount of energy per unit time, $E_{EP}$, and the number of EPs produced by each cell, $n_{EP}$, in a given time step is determined based on an estimate of the reaction rate within that cell.

### 2.4. Reaction rate, mass loss rate and heat release rate

In each burning cell, the local reaction rate (average reaction rate within the cell) is described in terms of the change in bulk density of fine fuel particles, $\rho_f$, with time and is captured by the following equation.

$$\frac{\partial \rho_f}{\partial t} = C_m \rho_f \rho_o \psi \sigma \lambda$$

where $C_m$ is a dimensionless reaction rate constant, $\rho_f$ and $\rho_o$ are the local bulk density [kg $m^{-3}$] of fine solid fuel (fine-scale biomass particles such as foliage or small twigs) and oxygen respectively. $\psi$ is the fraction of the fuel in the computational cell that is actively burning, $\sigma$ is the turbulent mixing coefficient, and $\lambda$ is the dimensionless stoichiometry factor. The oxygen density is modeled based on the local reaction rate through the following expression:

$$\rho_o = \rho_{gas}\left((0.21 - \gamma_{o,floor})e^{-C_{o2}\frac{\frac{\partial \rho_f}{\partial t}*N_{o2}*vol}{\sigma}} + \gamma_{o,floor}\right)$$

where $\rho_{gas}$ is the combined density of the all gases in a computational cell.$\gamma_{o,floor}$ is an assumed minimum bulk oxygen concentration that is possible within a burning cell and is set to 0.1 kg $O_2$/kg air but could be adjusted to be a function of Fire-CA cell volume,*vol*. The dimensionless

constant $C_{o2}$ in the exponential is initially set to 2 based on cursory analysis of CFD calculations, which will be refined through further explorations in subsequent studies. $N_{o2}$ is a stoichiometry coefficient normalized by the mass of the total products for oxygen in the combustion of wood in a simple wood burning model:

$$N_f(wood) + N_{o2}(oxygen) \rightarrow (products) + heat$$

This chemical equation involving a solid fuel and oxygen is a significant simplification compared to the multistage chain of reactions involving pyrolysis and many gas phase reactions and it should be noted that this approach assumes that the rate of combustion is mixing limited. The rate of pyrolysis is implicitly assumed to be limited by the availability of heat from the reaction, which is limited by the mixing processes bringing oxygen to the pyrolyzing fuel. The value of $N_{o2}$=.5448 and $N_f$=*.4552* based on Drysdale's (2011) stoichiometry for net combustion of wood. The stoichiometry factor, $\lambda$, is adjusted to prevent maximum burning with fuel or oxygen rich scenarios (Linn, 1997):

$$\lambda = \frac{\rho_f \rho_o}{\left(\frac{\rho_f}{N_f} + \frac{\rho_o}{N_{o2}}\right)^2}$$

The parameter $\psi$ is calculated based on the number of EPs, $n_{EP}$, that have been absorbed by dry fuel in the previous time step using the following relationship:

$$\psi = \frac{n_{EP} * E_{EP} * t_{burnout}}{\rho_f * vol * \left(H_{wood} - c_{p_{wood}}(T_{crit} - T_{ambient})\right)}$$

where $\psi$ is constrained to be between 0 and 1 and $E_{EP}$ is the energy per unit time per EP, which can be specified by the user. The value of $E_{EP}$ can be thought of as degree of energy resolution with large values leading to fewer EPs for the same reaction rate and thus less computational cost but the representation of the distribution of energy transferred to surroundings is reduced. Smaller values provide better finer grain representation of energy transport but add computational cost. $E_{EP}$ is set to 50 kW as a balance between computational cost and representation of the energy transport in the simulations for this manuscript. $t_{burnout}$ is the assumed time for fine fuel particles to burn out, which is currently estimated to be 30 s though the sensitivity of the modeled behavior to this parameter will be explored in future work. $T_{crit}$ and $T_{ambient}$ are the temperature [K] where fuel is assumed to combust and the ambient air respectively. $H_{wood}$ is the heat of combustion of wood, which is taken to be 18620 kJ kg$^{-1}$ (Drysdale, 2011) and $c_{p_{wood}}$ is the specific heat of wood, which is taken to be 1.7 kJ kg$^{-1}$ K$^{-1}$. The turbulent mixing parameter $\sigma$ is computed in a customary manner for turbulent diffusion coefficients:

$$\sigma = 0.09 s \rho_{gas} \sqrt{K}$$

where $\rho_{gas}$ is the density of the ambient air, while the length scale, $s$, and turbulent kinetic energy, $K$, are based on grid cell size and a Smagorinsky-style formulation following Germano et al. (1991). The reaction rate, $R$, explicitly describes the reduction in fuel within a computational cell [kg m$^{-3}$ s$^{-1}$] per computational time step, which is currently taken to be 1 s in the context of this text. The total energy release rate [kJ m$^{-3}$ s$^{-1}$], $\dot{q}_{Total}$, can be formulated in terms of the heat of combustion of wood, $H_{wood}$, $\dot{q}_{Total} = RH_{wood}$. Because it takes energy to heat fuel from ambient temperature to a nominal temperature of combustion, $T_{crit}$, we compute the net energy release from the fuel as: $\dot{q}_{net} = R(H_{wood} - c_{p_{wood}}(T_{crit} - T_{ambient}))$ A fraction of $\dot{q}_{net}$ is assumed to be lost upward to the distant atmosphere, $C_{rad\_loss}$, but to avoid a complex radiation calculation to determine the precise amount of energy lost to the sky versus absorbed by surroundings, we estimated $C_{rad\_loss}$ to be 0.2 (20% of the net energy.) This preliminary percentage estimate was based on consideration of radiation view factors and cursory examination of CFD calculations, further analysis of detailed physics calculations and experiments could be used estimate as a function of fire or environmental factors in the future. The number of EPs that are available to be transported to other locations is computed as:

$$n_{EP} = \frac{(1. - C_{rad\_loss}) * \dot{q}_{net}}{E_{EP}}$$

### 2.5. Transporting energy

Energy transfer to unburned fuel—and thus spreading fire—is accomplished by moving EPs from a location where they are produced to another location. Energy from wildfires is transported to surroundings through a variety of processes that occur over different scales. For the purposes of this simplified representation of the energy transport, the heat transfer processes are grouped into two different categories, which are referred to as 1) wind-dominated and 2) creeping. In the context of this model and this simplified categorization, the "wind-dominated" category is intended to capture the combined heating effects of convective bursts that blow transport heat in the direction of the local wind and radiative heating from flames that are also influenced by the local wind. This category of energy movement can be associated with fires in surface or elevated (shrubs or trees) fuels and is assumed to be the dominant mechanisms for head-fire spread. It is true that radiative heating is not constrained to the direction of the wind, but the radiative heating that is contrary to the wind direction is often not effective at spreading the fire since it is quickly offset by convective cooling. The "creeping" category includes the much slower influences of heat transfer processes occurring locally within the surface fuel beds including those associated with contact between adjacent fuel-particles and fine-scale mixing that happens within the fuel bed. These surface fire mechanisms are assumed in the model to be key factors in flanking and backing fire spread (portions of a fire moving perpendicular and contrary to the direction of fastest fire spread), and evaluated against high resolution observations of experimental burns in 2017–2018 at Tall Timbers Research Station (unpublished data) using methods similar to Loudermilk et al. (2014).

These two categories of heat transfer process, "wind-dominated" and "creeping," can be thought of as associated with fireline scales (on the order of the width of the fireline in the direction spread) or fuelbed scales (on the order of the depth of the surface fuel bed). These notional scale ranges are not mutually exclusive, and they depend on the fire environment as the high-intensity or wind-driven fires tend to have much wider or deeper firelines than low-intensity prescribed fires. However, fireline scales can be significantly larger than fuelbed scales and thus can contribute to much larger rates of fire spread.

The cellular automata aspect of this model represents the net influences of the movement of energy (by wind-dominated or creeping processes) through the transport of energy packets per unit time or EPs. EP's are simply a conceptualized quantity of energy that can move from one location to another per unit time. This could be the energy associated with hot gases or flames or radiant energy. Each EP represents a fixed amount of energy that is moved within a unit of time, $E_{EP}$, and they move through space, but are not associated with specific volumes. The notion of dilution or diffusion of energy as it moves away from its source is accomplished by decreasing the EP density per unit volume as distance from source increases. Since a typical power for an EP is 50 KW, there are often many of EPs being emitted in a given time step depending on the fire intensity at a given moment and location. Currently the transport rate or velocity of the EP while being transported is not computed and thus the EPs move from one location to another.

The movement of EPs associated with wind-dominated processes is achieved by deriving a direction and distance for the travel of each EP based on phenomenology observed in laboratory and field experiments as well as much higher fidelity coupled fire-atmosphere simulations. For each EP within a computational cell, a location for production is chosen randomly from within the zone that is taken to be actively burning within a computational cell (described in *Sub-grid zones: active fire, fuel*

*depletion, moisture depletion* subsection below). A possible length scale for the EP travel is estimated based on the observed flame length relationships described in Nelson et al. (2012). In order to use their relationship a local fire intensity is estimated by:

$$I = \frac{n_{EP} E_{EP}}{A_{active\_fire\_zone}}$$

where $A_{active\_fire\_zone}$ is the area of the sub-grid zone that is actively burning. The flame height is then estimated by:

$$h_{flame} = h_{fuel} + 0.0155 I^{\frac{2}{3}}$$

where $h_{fuel}$ is the height of the surface fuels and is taken to be zero for fuels in cells above the lowest vertical level. Nelson et al. (2012) also provided an expression for the fire updraft speed within a flame, $w^{'}$, which is not the same as a cell average vertical velocity:

$$w^{'} = 0.377 * I$$

The flame updraft speed, $w^{'}$, is concentrated in the location where the EP is emitted and is not necessarily the same as the plume velocity described above as the plume is associated with the collective buoyancy averaged over a cell. We used the flame height and fire updraft speed to estimate a length scale for the distance of heat transfer, $l$. In calculating $l$, we assume that the minimum length scale occurs at a horizontal wind speed of 0 but is stretched as horizontal wind components increases:

$$l = h_{flame} * MAXIMUM \left\{ 1, \sqrt{3} \left[ \frac{(u^2 + v^2)}{w^{'2}} \right]^{\frac{1}{4}} \right\}$$

where $u$ and $v$ are the local horizontal wind components. This expression is effectively the scaled square root of a convective Froude number. Using this expression when horizonal winds exceed three times the flame-induced vertical wind speed, the length scale starts to get stretched. Both the coefficient, $\sqrt{3}$, and the square root of the Froude number elements of this expression are preliminary and based on phenomenological expectations, but will be verified or refined through comparison with observations in future work. This length scale is used to describe the upper limit of the potential distance that an EP could move. The length scale is then adjusted based on whether it is more aligned with the horizontal or vertical winds and the magnitude of those winds:

$$l^{'} = l * \frac{2\left(\alpha_h w^{*} + \left(\frac{\pi}{2} - \alpha_h\right)\sqrt{u^2 + v^2}\right)}{\pi \sqrt{u^2 + v^2 + w^{*2}}}$$

where $\alpha_h$ is the angle of the EP trajectory with respect to the horizontal and is described below. In this equation, $w^{*}$ is a vertical wind component that is adjusted if only part of the cell is known to be on fire, factoring in for the concentration of an updraft. The distance that an EP moves is taken randomly from a triangular distribution ranging from 0 to $l$ (0 being the location of maximum probability). Thus, the travel distance for an EP, $d$, becomes:

$$d = l^{'} * \left(1 - \sqrt{1 - RND1}\right)$$

where RND1 as well as RND2, RND3, RND4, RND5 and RND6 below are a random number between 0 and 1, which are chosen for each EP. RND1 through RND4 are used at convective scales and RND 5 and RND6 are used at creeping scales (described below).

The EP trajectory angle relative to the x-axis in the horizontal plane, $\alpha_x$, is determined by adding a perturbation to the $u$ and $v$ wind components as illustrated in Fig. 2.

The strength of the perturbation is determined using a Gaussian distribution with a standard deviation of $\sqrt{K}/2$, where K is the local turbulent kinetic energy:

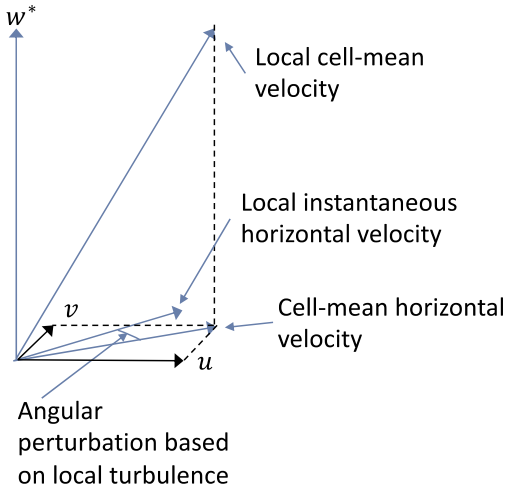


**Fig. 2.** An instantaneous local horizontal velocity is derived by combining the cell-averaged horizontal velocity components, $u$ and $v$, with $u$ and $v$ perturbations based on the local turbulence kinetic energy. This is combined with $w^{*}$ for a local instantaneous 3D wind speed.

$$\alpha_x = tan^{-1}\left( \frac{u + \frac{\sqrt{K}}{2} \mathrm{erf}(2 * RND2 - 1)}{v + \frac{\sqrt{K}}{2} \mathrm{erf}(2 * RND3 - 1)} \right)$$

Use of a Gaussian function to represent turbulent fluctuations within a forest canopy is an oversimplification as velocity distributions within forest canopies are known to be non-Gaussian and skewed (Shaw and Seginer, 1987; Mueller et al., 2014). Error induced by this oversimplification could be further amplified by the presence of a fire as Heilman et al. (2017) revealed that fires can further enhance the skewness of the velocity distributions. The Gaussian function was chosen for simplicity and evaluation of non-Gaussian velocity distributions will be investigated in future work.

The angle from the horizontal, $\alpha_h$, is determined by first computing a metric,$\phi$ , describing the local dominance of the fire-induced updraft over the horizontal wind.

$$\phi = \frac{w^{*}}{w^{*} + \sqrt{u^2 + v^2}}$$

$\phi$ approaches one when the updraft dominates over the horizontal wind and goes to zero when the horizontal wind is strong and the updraft is minimal. This metric is used to set the median angle of the EP trajectory above the horizontal plane, where the median EP trajectory is vertical when the updrafts dominate (see Fig. 3).

$$\alpha_h^{'} = \frac{\pi}{2} * \phi$$

Based on wind tunnel and field observations as well as high-fidelity simulations, the movement of heat from the active fire is heavily influenced by a tower and trough structure (Finney et al., 2015). The tower and trough structure tends to bifurcate the projection of the movement of hot air on a vertical plane aligned with $\alpha_x$ into two general paths, one with a strong horizontal component and one with a strong vertical component. The result is that heat advection from the fire often does not follow the median fireline wind trajectory, but instead follows either a path below the average trajectory or a more vertical path above the average trajectory. Based on this phenomenology as well as unsuccessful explorations where energy followed the median trajectory or local instantaneous mean wind direction, QUIC-Fire bifurcates the movement of heat along either of two paths based on the value of $\alpha_h^{'}$. In this initial

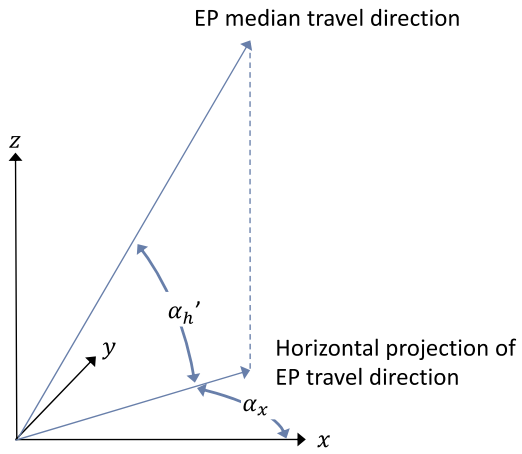


**Fig. 3.** The direction of the EP travel in relation to the coordinate axis. $\alpha_x$ is the angle between the horizontal projection of the EP travel direction and the x axis and $\alpha_h'$ is the median angle between the EP travel direction and the horizontal plane.

version of QUIC-Fire we have made the approximation that ratio of $\alpha_h'$ to vertical ($\pi/2$) determines the probability that an EP will follow a vertical path. Both this linear probability dependence function on $\alpha_h'$ and the strictly vertical and horizontal trajectories will be the subject of follow up research through detailed analysis of laboratory and field observations and CFD-based calculations, but for this preliminary version we use:

$$\alpha_h = \frac{\pi}{2} \; if \; \frac{2}{\pi}\alpha_h' + RND4 \geq 1 \; and \; \alpha_h = 0 \; if \; \frac{2}{\pi}\alpha_h' + RND4 < 1.$$

The transport of EPs to represent the creeping category of heat transfer process is meant to be only within the surface fuels and thus unlike the wind-dominated process model, the travel direction for "creeping" movement of EPs is currently constrained to be in a horizontal plane and only in the computational cells closest to the ground. The creeping travel distance and direction are estimated based on observations of some of the mechanisms by which flanking and backing fires spread: 1) short-duration turbulent fluctuations, 2) particle-to particle spread, and 3) small-scale reverse flows caused by turbulence driven by surface fuel roughness. The net result of these three mechanisms is a slow spread in directions that are not aligned with the mean wind. These are parameterized with the following expressions for the direction relative to the x coordinate axis, $\alpha_{x\_creep}$, creeping length scale, $l_{creep}$, and a triangular distribution of transport distances, $d_{creep}$, relative to the creeping length scale:

$$\alpha_{x\_creep} = 2\pi * RND5$$

$$l_{creep} = \frac{L_{creep}*}{2} dt \left(1 - \frac{u*cos(\alpha_{x\_creep}) + v*sin(\alpha_{x\_creep})}{\sqrt{u^2 + x^2}}\right)$$

$$d_{creep} = l_{creep}* \left(1 - \sqrt{RND6}\right)$$

The creeping length scale depends on a length scale parameter, $L_{creep}$, which is meant to be a function of the fuel bed geometry (height, packing ratio etc.) and turbulence intensity, but is currently estimated to be 2 m based loosely on the structure of grasses initially simulated and length/time scales of local wind fluctuations observed in backing fires. We intend to fully resolve this parameter in future versions of QUIC-Fire. The ratio in the parentheses is effectively the projection of the unit vector of the horizontal wind speed on the creeping direction and thus $l_{creep}$ is a maximum of 2 m when the creeping direction is in the opposite direction of the wind. With this formulation, $d_{creep}$ is chosen from a triangular distribution of the length scales ranging from 0 to $l_{creep}$ with the highest probability being 0.

### 2.6. Sub-grid zones: active fire, fuel depletion, moisture depletion

For QUIC-Fire to rapidly simulate fires on a landscape scale (kilometers to tens of kilometers) with minimal computational resources, we expect grid cell dimensions to be on the order of a meter or larger. This is not the minimum model resolution, but at finer scales the model would be unable to explicitly resolve the details of fire perimeters and fire widths of low intensity fires. Since our goal was to produce a model useful for prescribed fire, it was important to be able to adequately capture the behavior of low-intensity fires where the fire activity or fuel conditions are heterogeneous within computational cells. For this reason, QUIC-Fire models three subgrid spatial zones within each computational cell: the active fire zone, fuel depletion zone, and the moisture depletion zone (Fig. 4). For this initial version of the QUIC-Fire model, we described the zones in two horizontal dimensions (x and y). This simplification was made for computational ease because in our current application, the vertical dimensions were often about half the size of the horizontal grid dimensions (i.e., 2 × 2 × 1 m) and in cells closest to the ground, the fire and depletion activity were limited to the height of the fuels. It is important to note that by not tracking the vertical extent of the active fire zone, we were not adding the vertical cell dimension to our vertical energy transport as EPs were still emitted from random vertical positions from within the fuel bed. We will explore the implications of a three-dimensional zone description in future versions.

These zones, active fire, fuel depletion, and moisture depletion (shaded red, brown and grey in Fig. 4), were described with a zone center $(a_x, a_y)$, $(f_x, f_y)$, $(d_x, d_y)$ and a standard deviation in the x and y direction (indicated with $\sigma$ in Fig. 4. For simplification purposes, we assumed that within each of the three zones the associated properties of the fuels and fire activity were homogeneous. In other words, fuels and fuel moisture were homogenously distributed within their respective depletion zones. We also assumed that no fuel or moisture was depleted outside of their respective zones. Fire activity was treated as uniform within the active fire zone and thus EPs were assumed to be emitted from random locations within this zone.

These three zones are not mutually exclusive and in fact typically overlap as illustrated in Fig. 4. For example, when the fire EP lands in a cell, it will deplete some moisture. When a second EP lands in the cell (if it does not land in the same location) a new moisture depletion center and spatial standard deviation can be calculated based on the accumulating EP destination locations, thus creating a rectangular moisture depletion zone. As subsequent EPs are absorbed by the fuel in the cell where there is remaining moisture, the moisture depletion center is again adjusted along with the standard deviations, all the while tracking the total moisture that is evaporated from within the fuel depletion zone. Alternatively, if an EP is absorbed within the previously mapped out moisture depletion zone, one of two cases occurs: 1) more moisture is evaporated and the new destination point is used to update the moisture depletion zone center and standard deviations, or 2) the moisture is

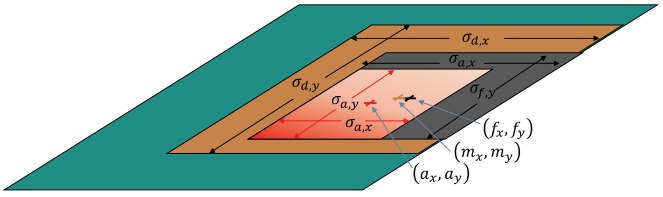


**Fig. 4.** Conceptual picture of nested active fire (red), fuel depletion (grey) and moisture depletion (brown) with a computational cell (green). In this case the fire might have spread in from the right of the cell near the center and is spreading to the left and towards the viewer in this image. (For interpretation of the references to colour in this figure legend, the reader is referred to the Web version of this article.)

completely depleted within this zone, in which case the moisture depletion zone is left unchanged, but the energy of the EP is used to consume some fuel and contribute to the development of the active fire zone. If EPs continue to land within the moisture depletion zone, eventually the moisture will be depleted within this zone and subsequent EPs can initiate active fire. This methodology would allow EPs being lofted short distances (compared to the width of a cell) into a cell, for example, from the right to develop a dry zone along the cells right side. Eventually it will be possible to develop an active fire zone that is entirely inside the moisture depletion zone. Once the active fire zone is established, EP's are emitted from this zone, which has the potential to send EPs beyond the current moisture depletion zone, further expanding it to the left. As solid fuel inside the active fire zone is consumed, a fuel depletion zone is established, creating a region where some but not all of the fuel has been consumed. The center and extent of the moisture and fuel depletion zones were calculated based on simple running statistics based on where the moisture and fuel depleting EPs land during the history of activity in a cell. The active burning region is more complex as fire activity is transient at any specific fire location. The center of the active fire zone is thus weighted most heavily by the locations where the heat release rate is greatest. When a new ignition location is established its heat release rate is approximated with an initial maximum followed by a linear decline with time over $t_{burnout}$.

The implications for this subgrid zone approach have yet to be fully explored, but they likely depend on the size of the cell in comparison to the energy transport distances or the depth of the fireline. For scenarios where the values of $l$ are on the same order or larger than the cell size, the zones can rapidly fill the entire cell as absorbed EPs are distributed widely across the cell. In this case the value modeling the three zones is minimal, but in scenarios where $l$ is small compared to the cell size, the zones will have more importance. The assumption of homogeneity within respective zones is the subject of ongoing discussions as it is certainly not applicable to all fuel beds. By using a more complicated distribution within each zone we would be able to represent the gradients within each zone, but at this point we believe that even with a top-hat distribution of depletions and fire activity within their zones, the subgrid heterogeneity provided by the zones themselves (in the zone or out of a zone) helps capture the impacts of some of the subgrid variability.

### 2.7. Fate of EP in QUIC-Fire

When an EP reaches its destination location, it evaporates moisture, ignites fuel in the new location, or heats the atmosphere. The fate of each EP is determined by the state of the destination fuel. A series of checks are performed regarding the probability of the presence of fuel and moisture level of the fuel.

Fuel densities and surface area per unit volume are used to determine the probability of an EP landing on viable fuel using the following equation.

$$P_{viable\ fuel} = \left[1 - e^{-\left(\frac{\rho_{f\_local}}{C_{igsc}} \frac{A_v}{A_{v\_norm} U_H^2} \left(U_H^2 + w^2\right)\right)}\right] * \frac{\rho_{f\_local}}{\rho_{f\_0}}$$

In this equation, $A_v$ is the surface area per unit volume of the local fuel and $A_{v\_norm}$ is a parameter used to normalize surface area per unit volume, such that $A_v/A_{v\_norm}$ is unitless. $A_{v\_norm}$ is currently chosen to be 4000 $m^{-1}$, which is a typical value for grass. $\rho_{f\_local}$ is the local bulk fuel density where the EP lands and $\rho_{f\_0}$ is the bulk density of the fuel in that computational cell at the beginning of the simulation. $U_H$ is horizontal wind velocity and $w$ is the local vertical velocity interpolated to cell centers. $C_{igsc}$ (kg $m^{-3}$) is a constant (currently set to 6 kg $m^{-3}$) that represents a theoretical density where the fuels are thick enough that an EP traveling 1 m through a cell with $A_v = A_{v\_norm}$ will a have 63% chance of being absorbed by fuel and not going to the atmosphere. This use of this constant can be thought of as the influence of the fuel density on the optical path length and on the spatial gradient of heat absorption into the fuel as hot gases blow through cooler fuel, both of which take on exponential forms under some circumstances. The value of $C_{igsc}$, which is currently set to 6 kg $m^{-3}$, does not currently have a firm basis yet but could be evaluated as part of future refinements. The portion of the equation in square brackets describes the effects local wind and fuel characteristics on the probability of the EP finding viable fuel if we assume that the fuels remain evenly distributed. This term describes something like the effects of fuel on mean free path of an EP. The factor on the right of the expression accounts for the increased spatial heterogeneity and gaps between fuel elements as the fuel gets depleted.

If the EP lands within the fuel depletion zone, then the locally depleted fuel density of the zone (fuel depletion concentrated in fuel depletion zone) is used as $\rho_{f\_local}$. As fuel is depleted in the depletion zone, its receptivity to new EPs approaches zero. If an EP does not get absorbed by the fuel, then its energy is released to the atmosphere and goes on to generate a buoyant plume.

If it is absorbed by fuel, then it can either heat/ignite some of the fuel or heat and evaporate water if the fuels at the destination are wet. If the ambient fuel bed is not completely dry (0% moisture) at the beginning of the simulation, the EP destination location will either fall within a moisture depletion zone or not. If the EP was absorbed by fuel outside the current moisture depletion zone, its energy will be used to heat a fraction of the moisture to vaporization. Additionally, the location of the EP within the cell was used to grow the moisture depletion zone of the cell. If an EP was absorbed by fuel inside the current moisture depletion zone, then its energy will be used to evaporate any water remaining within the zone. If there was no moisture within the zone, then the energy of the EP was used to ignite fuel and this was considered a successful ignition.

## 3. Simulations

To demonstrate model performance, we use two case study comparisons between FIRETEC and QUIC-Fire simulations. The goal of these comparisons is to assess if the reduced-order representations of processes and fire-atmospheric feedbacks in QUIC-Fire at cell levels aggregate to produce overall fire behavior and response to fire conditions that are like what a full CFD fire/atmosphere model provides. One advantage to comparing QUIC-Fire with FIRETEC is that they rely on nearly identical 3D representations of vegetation in the fuelbed, allowing for direct comparison of outputs to the CFD-based FIRETEC model.

### 3.1. Case study 1: long line vs. short line ignition

Linn and Cunningham (2005)—hereafter, LC2005—conducted a series of simulations using HIGRAD/FIRETEC to investigate how fire behavior in grasslands was influenced by the initial length of the fireline and the ambient winds. Initial line length was found to influence both the rate of spread and fire shape due to differences in the coupled fire-atmosphere interactions. Overall the head fire spread rates of LC2005 were found to be in good agreement with both field experiments (Cheney and Gould, 1995; Cheney et al., 1993) and empirical model estimates (Cheney et al., 1998). The simulations of LC2005 provide an ideal test case for initial evaluation of whether the simplified representations of local fire phenomena in QUIC-Fire combine to capture reasonable overall fire-atmosphere feedbacks and thus fire behavior as they provide a very simple fire environment that highlights the role of fire-atmosphere coupling.

For the simulations of LC2005, a domain of uniform fuels with no topographic slope was used. The fuels represented tall grass with a height of 0.7 m and an aerial distribution of 0.7 kg $m^{-2}$. The computational domain was discretized into a uniform horizontal grid of 400 m × 400 m with 2 m horizontal resolution and a stretched vertical grid

with the near ground spacing starting at 1 m and stretching to 25 m spacing at a height of 150 m. The initial fuel moisture fraction (i.e., the mass of water divided by the mass of fuel) was specified as 0.05.

In the QUIC-Fire simulation, ambient winds are prescribed to be in the positive x direction and are initialized with a log profile that assumes neutral atmospheric stability. For this study we consider wind speeds of 1, 3, 6, and 12 m $s^{-1}$ as measured at a height of 10 m. In LC2005 the initial and inflow profiles are of the same speeds but a uniform profile was assumed, and vegetative drag could develop the near-surface shear layer. To account for potential differences between our log profile and the profile of LC2005 we used mid-flame wind speeds reported in LC2005 and adjust these to a reference height of 10 m using a log profile using a roughness length of 0.1 m for tall grass.

We consider ignition line lengths of 16 and 100 m, hereafter referred to as short and long lines respectively. For QUIC-Fire, ignition was accomplished by removing any moisture and adding energy to the grid cells designated for ignition. For these cases the amount of energy added was 2 EPs. In LC2005, ignition was accomplished by removing any initial fuel moisture from the ignition cells and increasing the temperature from 300 K to 1000 K over a span of 2 s. Difference in ignition method should only impact very early stages of fire spread, and thus we focus comparisons on times after the first 60 s of spread.

### 3.2. Case study 2: prescribed fire multiline ignition

To demonstrate QUIC-Fire's ability to work with three dimensional fuels and complex ignition patterns, we simulated a typical burn pattern for a prescribed fire at Eglin Air Force Base (EAFB), ignited by 5 strip head fire ignition lines moving perpendicular to the wind direction. The rates of ignition across the unit reflect EAFB use of all-terrain vehicles (ATVs) to ignite units of this size. The 3D fuels were parameterized for fire-maintained longleaf pine (*Pinus Palustris*)-turkey oak (*Quercus laevis*) sandhill ecosystems using fire effects monitoring data (Hiers et al., 2007) and supplemented by fuel data from the Prescribed Fire Combustion and Atmospheric Dynamics Experiment (RxCADRE; Ottmar et al., 2016).

We analyze each simulation for fuel consumption in different forest strata which are common foundational data for prescribed fire objectives. The burn unit modeled for this comparison was 40 ha, with full model domain extending 500 m × 1200 m in planer dimensions and 614 m in height with 2 m horizontal resolution and 1 m vertical resolution. We define surface fuels as those fuels in the lower most model layer (height < 1.5 m), midstory fuels occupy layers 2–5 (height 1.5–3 m), and canopy fuels as any fuels above layer 3 (height > 3 m). This simulation was compared with FIRETEC using the same fuel inputs, ignition pattern, rate of ignition, and mean input windspeed of 5 m $s^{-1}$.

## 4. Results

### 4.1. Comparisons to grass fires

Fire perimeters as a function of time for wind speeds of 1, 3, 6, and

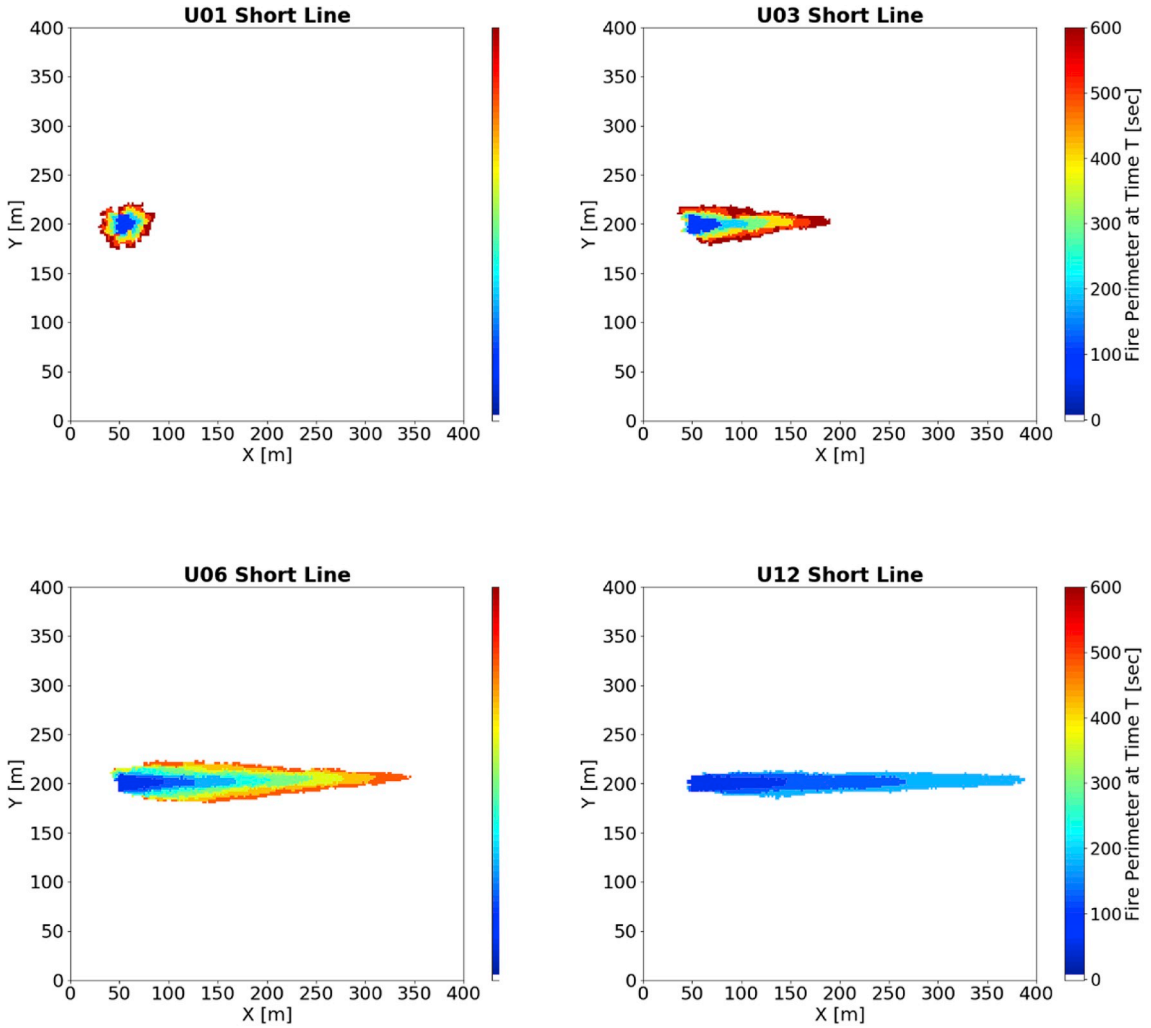


**Fig. 5.** Fire perimeter progression for short line ignitions and wind speeds of 1, 3, 6, and 12 m $s^{-1}$.

12 m $s^{-1}$ are shown in Figs. 5 and 6 for the short and long line cases respectively. For the short ignition line and 1 m $s^{-1}$ winds (upper left panel of Fig. 2), the pattern of fire spread is predominantly circular and as wind speeds increase the fire perimeters become elongated and focused to a sharp point downwind of the ignition. The longer ignition lines in Fig. 6 lack the circular pattern at low speeds and have a more lobed pattern due to increased competition for indrafts to feed the larger number of updrafts required for the longer line.

Fig. 7 shows the downwind propagation of the fire front with time for the short line cases for the QUIC-Fire simulations. Spread rates are nearly constant for each wind speed after a period of adjustment during the first 60 s as the initial ignition line builds into a sustainable fire front. The impact of this adjustment period on rate of spread was evident when estimated via a linear fit, as performed in LC2005 (Table 1). Limiting the data in the linear fit to the period after the 60 s adjustment period improves the agreement with LC2005 spread rates for the 1 and 12 m $s^{-1}$ cases.

The long line cases also exhibit near constant spread rates outside of the ignition influenced period (Fig. 8). As for the short line cases, the QUIC-Fire simulation spread rates are slower than those of LC2005 (Table 2). Adjusting the log wind profile used in QUIC-Fire such that the near surface winds more closely match the winds in the lowest model level of LC2005 greatly reduces the differences in spread rates for the higher wind speed cases. The adjusted 10-m wind speeds are 1.1, 3.5, 7.6, and 14.5 m $s^{-1}$. While adjusting the wind profile improves the agreement between QUIC-Fire and LC2005, other sources of potential

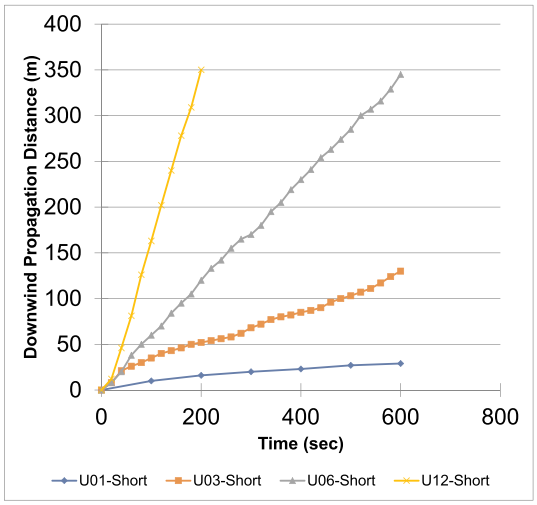


**Fig. 7.** QUIC-Fire modeled downwind propagation distance as a function of time for the "short line" cases at wind speeds of 1, 3, 6, and 12 m $s^{-1}$. Distance was recorded every 20 s except for 1 m $s^{-1}$ case where measurement interval was 100 s.

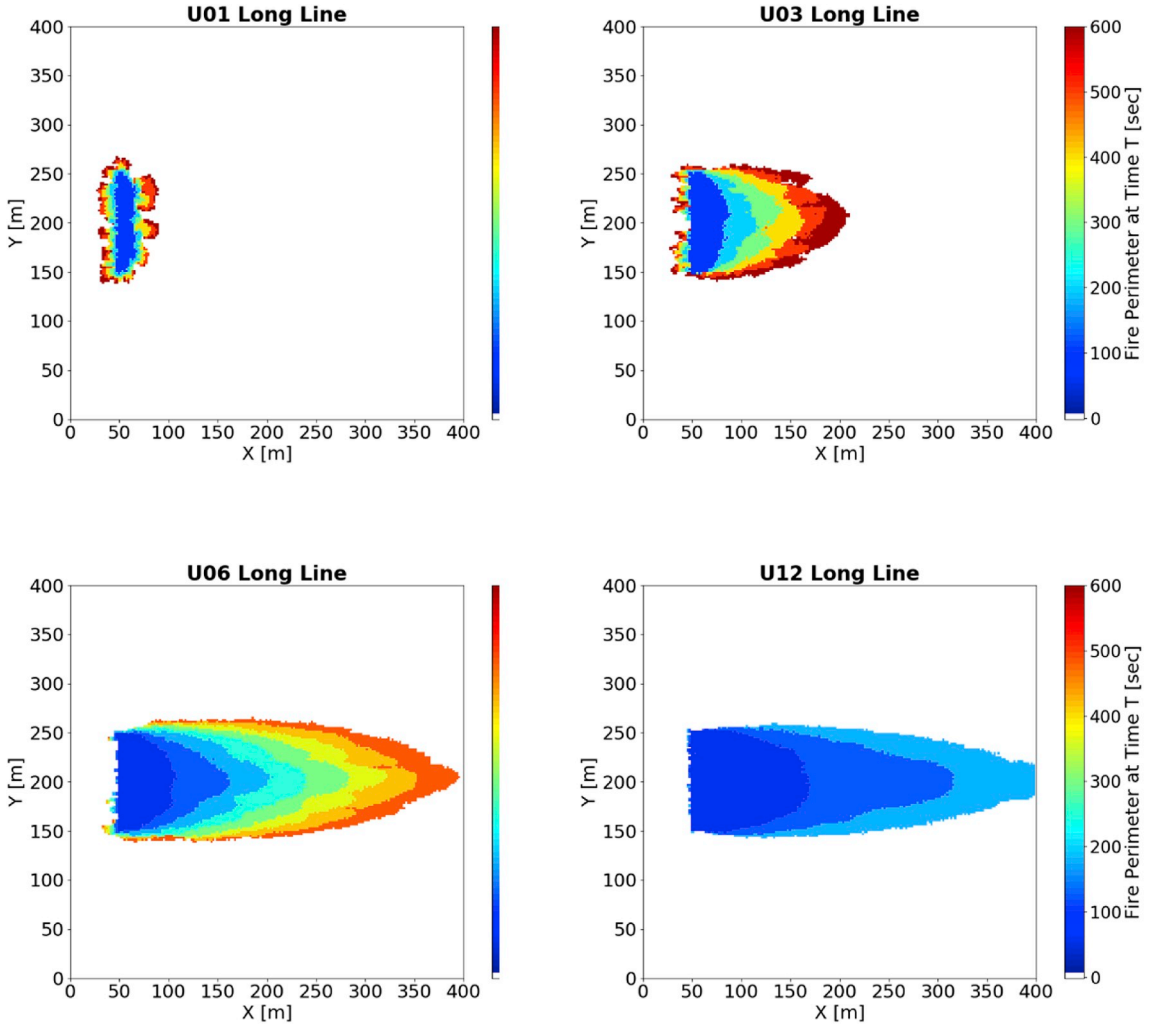


**Fig. 6.** Fire perimeter progression for long line ignitions and wind speeds of 1, 3, 6, and 12 m $s^{-1}$.

**Table 1**
Comparison of spread rates (m $s^{-1}$) for Short Line Ignitions as a function of wind speed using FIRETEC results from LC2005 and QUIC-Fire average results and results following initial 60 s of model runs (60+).

| | Windspeed (m $s^{-1}$) | | | |
|---|---|---|---|---|
| **Model Run** | 1 m $s^{-1}$ | 3 m $s^{-1}$ | 6 m $s^{-1}$ | 12 m $s^{-1}$ |
| LC2005 | 0.1 | 0.26 | 0.76 | 2.41 |
| QUIC-Fire-avg | 0.048 | 0.22 | 0.58 | 1.75 |
| QUIC-Fire-60+ | 0.08 | 0.19 | 0.59 | 1.92 |

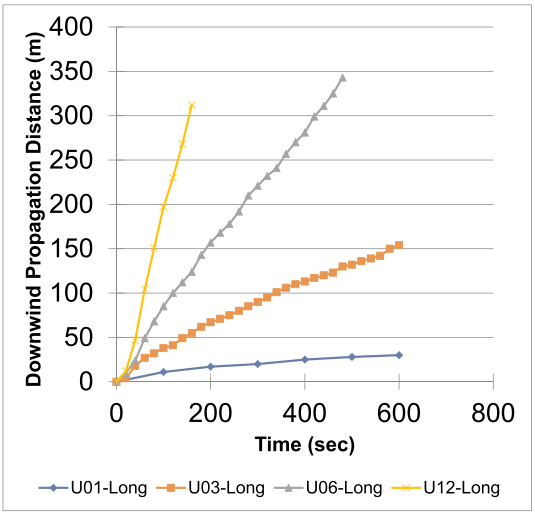


**Fig. 8.** QUIC-Fire modeled downwind propagation distance as a function of time for the "long line" cases at wind speeds of 1, 3, 6, and 12 m $s^{-1}$. Distance was recorded every 20 s except for 1 m $s^{-1}$ case where measurement interval was 100 s.

**Table 2**
Comparison of spread rates (m $s^{-1}$) for Long Line Ignitions as a function of wind speed using FIRETEC results from LC2005 and QUIC-Fire average results and results following initial 60 s of model runs (60+).

| | Windspeed (m $s^{-1}$) | | | |
|---|---|---|---|---|
| **Model Run** | 1 m $s^{-1}$ | 3 m $s^{-1}$ | 6 m $s^{-1}$ | 12 m $s^{-1}$ |
| LC2005 | 0.27 | 0.79 | 1.37 | 3.22 |
| QUIC-Fire-avg | 0.050 | 0.26 | 0.71 | 1.95 |
| QUIC-Fire-60+ | 0.050 | 0.24 | 0.73 | 2.21 |
| QUIC-Fire-60 + Adj Profile | 0.055 | 0.30 | 1.03 | 2.95 |

disagreement such as differences in turbulence levels are not as easily adjusted.

Overall the QUIC-Fire results are consistent with those of LC2005 in that longer ignition lines result in faster rates of spread than shorter lines for a given wind speed. As noted above, the results of LC2005 are generally consistent with the field experiments described by Cheney et al. (1993) and Cheney and Gould (1995). The one exception to this consistency was LC2005 finding the influence of line length being stronger for lower winds where Cheney and Gould (1995) indicate that the effect was greatest at high winds. Low wind speeds are where QUIC-Fire and LC2005 differ the greatest, with QUIC-Fire response to line length being weaker at low winds than LC2005 (Table 3). This result, however, shows QUIC-Fire simulations to be more consistent with the findings of Cheney and Gould (1995).

Lateral spread was significantly higher in QUIC-Fire than LC2005. While LC2005 yielded length-to-breadth ratios lower than those of Alexander (1985), discrepancies were potentially attributable to an overly simplified treatment of radiation or turbulent heat exchange, or under-resolution of the fuel bed. Unlike LC2005, QUIC-Fire yielded

**Table 3**
Ratio of spread rates for Long Line Ignitions to Short Line Ignitions as a function of wind speed.

| | Windspeed (m $s^{-1}$) | | | |
|---|---|---|---|---|
| **Model Run** | 1 m $s^{-1}$ | 3 m $s^{-1}$ | 6 m $s^{-1}$ | 12 m $s^{-1}$ |
| LC2005 | 2.70 | 3.04 | 1.80 | 1.34 |
| QUIC-Fire-60 + Adj Profile | 1.14 | 1.54 | 1.78 | 1.55 |

length-to-breadth ratios larger than those of Alexander (1985). The low lateral spread rates from QUIC-Fire could be caused by the absence of natural variability in the input wind field, which was artificially constrained in these comparisons. Alternatively, the low lateral spread rates from QUIC-Fire could also be a manifestation of our assumed Gaussian and isotropic velocity distributions. As Alexander (1985) does not provide variability statistics on winds, it was difficult to replicate subtle but potentially important variation driving lateral spread.

### 4.2. *Prescribed fire multiline ignition*

Simulation of an operational prescribed fire using multiple ignition lines shows good qualitative agreement between QUIC-Fire and FIRETEC (Fig. 9). Five firelines were ignited in the simulation moving from right to left in Fig. 9 and the ambient wind of 5 m $s^{-1}$ was blowing from the image foreground towards the background. After 120 s of simulation time (top 2 images in Fig. 9) the surface fire was beginning to ignite the midstory as ignition lines converge to create strong convective updrafts. By 300 s (bottom 2 images in Fig. 9) the fire was actively consuming fuel within all three fuel strata. By 420 s (not shown) consumption rates decline as fire from early in the simulation entered a smoldering phase and the left flank continues flaming combustion within the last zone of merged firelines.

Overall in the QUIC-Fire simulation 98.6% of surface fuels were consumed along with 33.6% of the canopy. Here surface fuels are those fuels within the first vertical level of the model and canopy fuels are those fuels above the fifth vertical level. These consumption values are considered typical for aggressive ignition patterns like strip head fire that target midstory consumption and often at the expense of some canopy consumption (Ottmar et al., 2016). Comparison of fuel consumption time series with the FIRETEC simulations reveal similar trends (Fig. 10). FIRETEC ramps up to a constant rate of consumption for surface fuels more quickly than QUIC-Fire but the rates of consumption are similar and the overall difference in the percentage of fuel consumed is only 3.2%. For canopy consumption FIRETEC is again quicker to initiate canopy consumption but the rates and total consumption are quite similar for QUIC-Fire, differing by 2.6% in total canopy consumed.

## 5. Discussion

The new coupled fire-fuel-atmosphere model QUIC-Fire shows great promise as an emerging planning tool for complex ignitions. As these two test case studies illustrate, QUIC-Fire is capable of faster than real time simulations of complex fire-atmospheric feedbacks resulting from variation in ignition patterns and produced results like the CFD solution for these scenarios at ~1/2000 the computational cost.

Due to nearly identical fuel inputs, QUIC-Fire performance can be analyzed against the numerical CFD model HIGRAD/FIRETEC. Under a range of wind speed conditions in these two ignition line length scenarios, QUIC-Fire showed similar trends to the FIRETEC spread rates. While its performance diverged at lower windspeeds, its results showed closer agreement than FIRETEC to empirical data on which the LC2005 simulation was built (Cheney et al., 1993). This realistic representation of the interaction of wind speed, length of ignition line, and fire spread was a critical test of the ability of QUIC-Fire to capture basic phenomena that emerge from coupled fire-atmospheric processes.

The comparison of QUIC-Fire to FIRETEC using a complex ignition

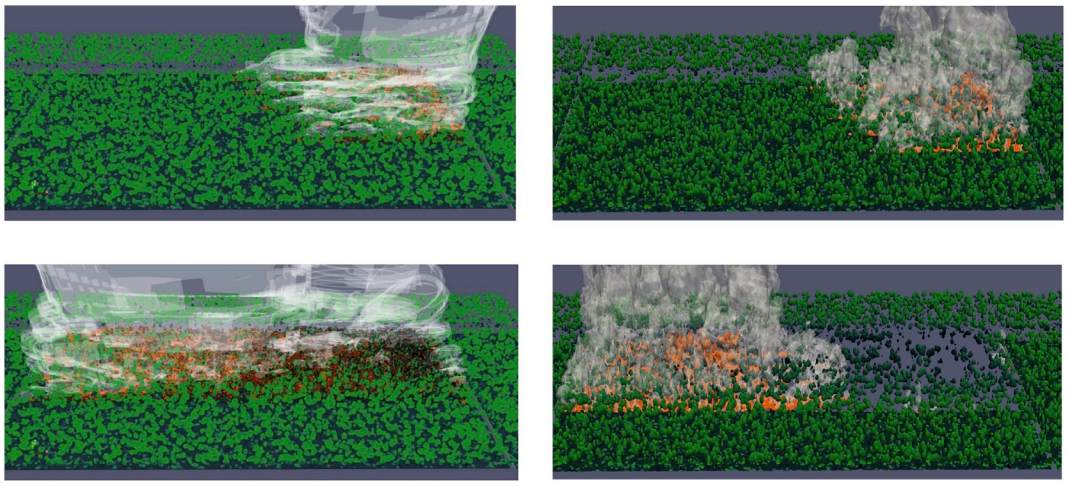

**Fig. 9.** Orthogonal view of QUIC-Fire (left) and FIRETEC (right) simulation of Eglin AFB prescribed burn at 120 and 300 s (top and bottom). Five staggered ignition lines were ignited (from right to left) at rates typical of all-terrain vehicle ignitions at Eglin. Green iso-surfaces are vegetation density, oranges are mass loss rate, and white shades indicate locations of rising plumes. (For interpretation of the references to colour in this figure legend, the reader is referred to the Web version of this article.)

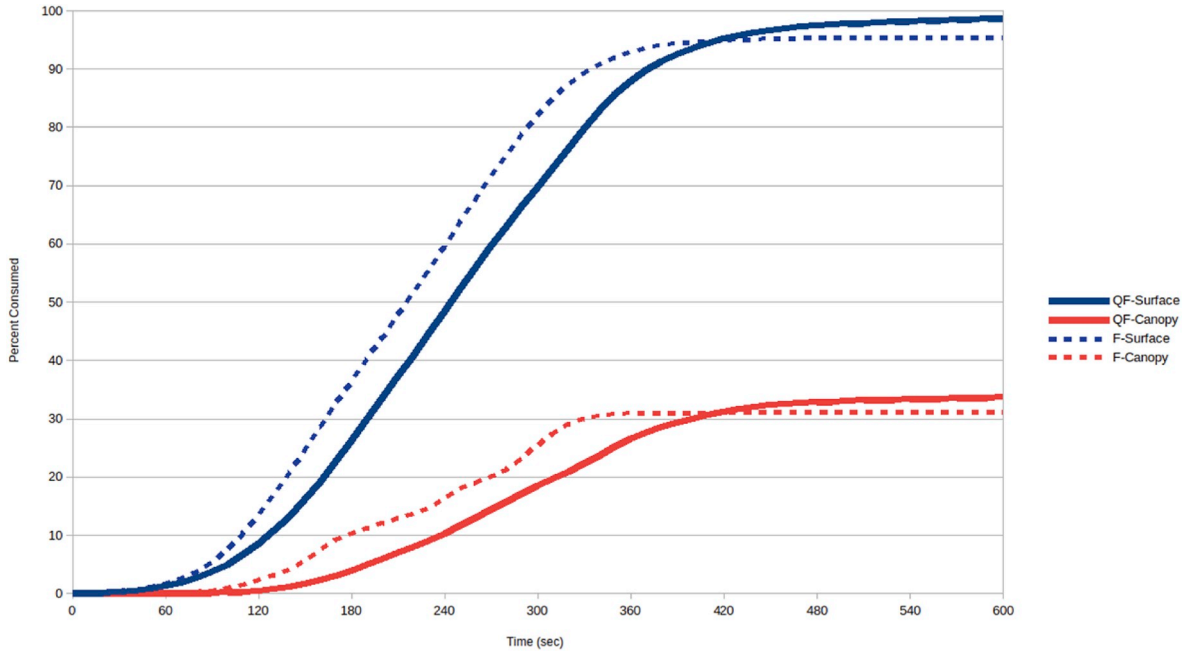


**Fig. 10.** Percent mass consumed within surface and canopy fuels as a function of time for QUIC-Fire (QF) and FIRETEC (F).

pattern common for prescribed fire operations in the southeastern United States further illustrates potential utility in capturing altered flows resulting from both the 3D fuel structure and the fire-induced buoyant plume. In planning prescribed fires, a manager routinely relies upon experience to distill what combination of ranges of wind speeds, fuel moistures, and ignitions patterns yield fire intensities that are suitable for achieving desirable ecological outcomes. Models commonly used in prescription development (NWCG, 2017) cannot account for the multiple interacting firelines associated with most prescribed fire ignitions as they assume free-burning fire (Yedinak et al., 2018). Interacting firelines on prescribed fires drive areas of enhanced convection that migrate progressively across the burn unit forming complex patterns as firelines merge and burn out. This simulation shows the promise of QUIC-Fire to rapidly account for how winds, fuel conditions, and ignition pattern interact to develop a complex mosaic of fire interactions across a burn unit.

For models to be useful in evaluating prescribed fire ignition scenarios, the impacts of the fire-atmosphere interaction must be effectively resolved. In Scenario 2, the convection convergence driven by interacting firelines was similarly represented by both QUIC-Fire and FIRETEC. Put simply, as heated air parcels rise above the fires, other air parcels were drawn towards the rising air to fill the volume vacated by the rising air. As intensity increased, greater volumes of air were pulled in under the rising plume. Nearby fires pulled on one another, with the net effect that different firelines were drawn together. In addition, it should be noted that the fire-generated flow is not aligned with the mean ambient wind flow. This phenomenon must be adequately described in terms of the underlying fire dynamics for a model to be useful in situations where complex patterns of multiple firelines exist, such as most prescribed fires. In addition to being able to capture the impact of heterogeneous and dynamically placed ignitions, QUIC-Fire accounted for influences of fuel structure and ambient winds that change during the

course a fire.

Despite the recent focus of fire science on the importance of convective heat transfer (Canfield et al., 2014; Finney et al., 2015), only CFD representations could reliably capture buoyancy-driven fire-atmospheric feedbacks (Linn and Cunningham, 2005; Mell et al., 2009; Parsons et al., 2011). Yet, such tools remain inaccessible due to intense computational demands and are largely applied in research contexts (Cruz and Alexander, 2012; Mell et al., 2018; Sullivan, 2009a). Thus, managers continually rely on radiation driven semi-empirical fire spread models for operational planning (Andrews, 1986; Finney, 1998; Tymstra et al., 2010) that were originally designed to predict forward fire spread and employed in evaluating firefighter safety. Unfortunately, these types of operational models are inappropriate for prescribed fire scenarios where the importance of fire-atmosphere interaction is amplified.

Both prescribed fire ignition patterns and wildfire tactical ignitions are determined primarily by highly variable wind fields and fuel characteristics (e.g., moisture content and loading), all of which change in both space and time (Heilman et al., 2015). It is also common for prescribed fires to be performed in the context of high structural variability in vegetation that occurs across scales (Furman, 2018). For example, both fine-scale fuel breaks and adjacent large burned areas can alter patterns of air flow and can facilitate enhanced inflows that have a large impact on fire behavior (Linn et al., 2012). Alternatively, planned burned units are often bordered by denser vegetation, which is more resistant to ambient wind flows and alters patterns of fire spread (Lashley et al., 2014). The combined effects of vegetation structural influences on wind will influence fire behavior in ways that may help or hinder in meeting burn objectives, therefore, a useful model must be able to account for the effects of vegetation on both fuels and wind flows. While QUIC-Fire does not include a detailed treatment of the turbulent processes associated with vegetation or fire, it has compared favorably to the more physically detailed FIRETEC model and thus shows potential for being a useful tool for fire managers.

QUIC-Fire represents a critical innovation in efforts to create a prescribed fire modeling tool that could be widely applied by fire managers including the essential coupled fire-atmospheric interaction without large computational demands. QUIC-Fire provides the ability to manipulate fuels, winds, and ignition patterns and then compare predicted fire behavior among those scenarios. The computational efficiency allows for ensemble runs to explore, for example, fire behavior predictions resulting from variations in wind speed, gustiness, or fuel moisture. The reliance on 3D fuels already available for FIRETEC is a critical strength of this tool, as QUIC-Fire predictions can be tested against a CFD model solution to examine the underlying physics when predictions do not match expectations.

## 6. Conclusions

Here we describe the conceptual basis, basic formulation, and initial demonstration of a new fast-running modeling tool, QUIC-Fire, that can be applied to prescribed fire planning. QUIC-Fire is the integration of a phenomenologically based fire spread model with the fast running wind solver QUIC-URB and provides a self-determining fire prediction capability that represents the critical coupled fire-atmosphere feedbacks at scales relevant for prescribed fire. Although the development of this model is in the nascent stages of development, initial results show an encouraging capability to capture basic trends in fire behavior, response of fire spread to size of fire, and consumption of canopy fuels in prescribed fire scenarios. Based on the results of this initial assessment, the combination of the QUIC-URB wind solver with a phenomenologically based cellular automata approach to modeling the fire spread shows promising potential and warrants continued development.

QUIC-Fire is currently being used for simulations of fire on relatively flat terrains and most prescribed fires in the US occur under minimal topographic relief (Melvin, 2015). However, current efforts to adapt this coupled fire-atmospheric modeling framework for topography are expected to extend QUIC-Fire's application to prescribed fire in complex terrain. QUIC-Fire's ability to represent fire-atmospheric feedbacks, such as those that govern prescribed fire behavior at relevant scales, while running on a basic laptop is intended to begin providing a capability for a broader set of users to explore prescribed fire behavior. Its ability to model response to both ignition patterns and a temporally and spatially variable fire environment without computational expense of CFD solutions is a critical design feature. Advancing this initial effort, however, will require continued refinement and validation against observations. For example, the representation of near-fire turbulence as influenced by ambient winds, vegetation and the fire itself is a focus of model advancement efforts (ambient and fire influenced) as the limitations of the current Smagorinsky-style approach could have implications for the model's representation of fires in some circumstances. Additionally, efforts to refine representations of heat transfer length scales, directions and efficiency, representation of backing and flanking fire spread phenomenology, as well as vegetation drag and fire/atmosphere feedbacks will continue.

## Declaration of competing interest

Authors declare no conflicts of interest.

## Aknowledgements

Funding was provided in part by the Department of Defense through the Strategic Environmental Research and Development Program project RC-2643 and Environmental Security Technology Certification Program project RC-201303, the Los Alamos National Laboratory LDRD program, the USDA Forest Service Southern Research Station, USDA Forest Service Rocky Mountain Research Station, and USDA Forest Service R&D Washington Office through the National Fire Plan and Tall Timbers Research Station. We are appreciative of the efforts of James Furman, Brett Williams, and participants in the Prescribed Fire Science Consortium for their support and encouragement in developing this tool.

## Appendix A. Supplementary data

Supplementary data to this article can be found online at https://doi.org/10.1016/j.envsoft.2019.104616.

## References

Achtemeier, G.L., 2013. Field validation of a free-agent cellular automata model of fire spread with fire–atmosphere coupling. Int. J. Wildland Fire 22, 148–156.
Achtemeier, G.L., Goodrick, S.A., Liu, Y., 2012. Modeling multiple-core updraft plume rise for an aerial ignition prescribed burn by coupling Daysmoke with a cellular automata fire model. Atmosphere 3 (3), 352–376.
Alexander, M., 1985. Estimating the length-to-breadth ratio of elliptical forest fire patterns. In: Proceedings of the Eighth Conference on Fire and Forest Meteorology. Soc. Am. For, Bethesda, MD, 85-04.
Andrews, P.L., 1986. BEHAVE: Fire Behavior Prediction and Fuel Modeling System-BURN Subsystem, Part 1.
Bond, W.J., Keeley, J.E., 2005. Fire as a global 'herbivore': the ecology and evolution of flammable ecosystems. Trends Ecol. Evol. 20 (7), 387–394.
Canfield, J., Linn, R., Sauer, J., Finney, M., Forthofer, J., 2014. A numerical investigation of the interplay between fireline length, geometry, and rate of spread. Agric. For. Meteorol. 189, 48–59.
Cionco, R.M., 1965. A mathematical model for air flow in a vegetative canopy. J. Appl. Meteorol. 4 (4), 517–522.
Cheney, N., Gould, J., 1995. Fire growth in grassland fuels. Int. J. Wildland Fire 5 (4), 237–247.
Cheney, N., Gould, J., Catchpole, W., 1993. The influence of fuel, weather and fire shape variables on fire-spread in grasslands. Int. J. Wildland Fire 3 (1), 31–44.
Cheney, N., Gould, J., Catchpole, W.R., 1998. Prediction of fire spread in grasslands. Int. J. Wildland Fire 8 (1), 1–13.
Chiodi, A., Larkin, N., Varner, J.M., 2018. An analysis of Southeastern US prescribed burn weather windows: seasonal variability and El Niño associations. Int. J. Wildland Fire 27 (3), 176–189.
Coen, J., 2013. Modeling Wildland Fires: A Description of the Coupled Atmosphere-Wildland Fire Environment Model (CAWFE).

Coen, J.L., Cameron, M., Michalakes, J., Patton, E.G., Riggan, P.J., Yedinak, K.M., 2013. WRF-Fire: coupled weather–wildland fire modeling with the weather research and forecasting model. J. Appl.Meteorol. Climatol. 52 (1), 16–38.
Cruz, M.G., Alexander, M.E., 2012. Evaluating regression model estimates of canopy fuel stratum characteristics in four crown fire-prone fuel types in western North America. Int. J. Wildland Fire 21 (2), 168–179.
Cruz, M.G., Alexander, M.E., 2019. The 10% wind speed rule of thumb for estimating a wildfire's forward rate of spread in forests and shrublands. Ann. For. Sci. 76 (2), 44.
Davidson, G., 1989. Simultaneous trajectory and dilution predictions from a simple integral plume model. Atmos. Environ. 23 (2), 341–349, 1967.
Drysdale, D., 2011. An Introduction to Fire Dynamics. John Wiley & Sons.
Finney, M.A., 1998. FARSITE: Fire Area Simulator-Model Development and Evaluation. In: Res. Pap. RMRS-RP-4, vol. 47. US Department of Agriculture, Forest Service, Rocky Mountain Research Station, Ogden, UT, p. 4. Revised 2004.
Finney, M.A., Cohen, J.D., Forthofer, J.M., McAllister, S.S., Gollner, M.J., Gorham, D.J., Saito, K., Akafuah, N.K., Adam, B.A., English, J.D., 2015. Role of buoyant flame dynamics in wildfire spread. Proc. Natl. Acad. Sci. 112 (32), 9833–9838.
Furman, J., 2018. Next generation fire modeling for advanced wildland fire training. Fire Manag. Today 78 (4), 48–53.
Germano, M., Piomelli, U., Moin, P., Cabot, W.H., 1991. A dynamic subgrid-scale eddy viscosity model. Phys. Fluids A Fluid Dyn. 3, 1760–1765.
Guyette, R., Stambaugh, M.C., Dey, D., Muzika, R.M., 2017. The theory, direction, and magnitude of ecosystem fire probability as constrained by precipitation and temperature. PLoS One 12 (7), e0180956.
Heilman, W.E., Bian, X., Clark, K.L., Skowronski, N.S., Hom, J.L., Gallagher, M.R., 2017. Atmospheric turbulence observations in the vicinity of surface fires in forested environments. J. Appl. Meteor. Climatol. 56, 3133–3150.
Heilman, W.E., Clements, C.B., Seto, D., Bian, X., Clark, K.L., Skowronski, N.S., Hom, J. L., 2015. Observations of fire-induced turbulence regimes during low-intensity wildland fires in forested environments: implications for smoke dispersion. Atmos. Sci. Lett. 16 (4), 453–460.
Hiers, J.K., O'Brien, J.J., Mitchell, R.J., Grego, J.M., Loudermilk, E.L., 2009. The wildland fuel cell concept: an approach to characterize fine-scale variation in fuels and fire in frequently burned longleaf pine forests. Int. J. Wildland Fire 18 (3), 315–325.
Hiers, J.K., O'Brien, J.J., Will, R.E., Mitchell, R.J., 2007. Forest floor depth mediates understory vigor in xeric *Pinus palustris* ecosystems. Ecol. Appl. 17 (3), 806–814.
Hilton, J., Miller, C., Sullivan, A., Rucinski, C., 2015. Effects of spatial and temporal variation in environmental conditions on simulation of wildfire spread. Environ. Model. Softw 67, 118–127.
Hilton, J., Sullivan, A.L., Swedosh, W., Sharples, J., Thomas, C., 2018. Incorporating convective feedback in wildfire simulations using pyrogenic potential. Environ. Model. Softw 107, 12–24.
Hoffman, C., Sieg, C., Linn, R., Mell, W., Parsons, R., Ziegler, J., Hiers, J., 2018. Advancing the science of wildland fire dynamics using process-based models. Fire 1 (2), 32.
Ichoku, C., Giglio, L., Wooster, M.J., Remer, L.A., 2008. Global characterization of biomass-burning patterns using satellite measurements of fire radiative energy. Remote Sens. Environ. 112 (6), 2950–2962.
Lai, C.C., Lee, J.H., 2012. Mixing of inclined dense jets in stationary ambient. J. Hydro-Environ. Res. 6 (1), 9–28.
Lashley, M.A., Chitwood, M.C., Prince, A., Elfelt, M.B., Kilburg, E.L., DePerno, C.S., Moorman, C.E., 2014. Subtle effects of a managed fire regime: a case study in the longleaf pine ecosystem. Ecol. Indicat. 38, 212–217.
Linn, R., Canfield, J., Cunningham, P., Edminster, C., Dupuy, J.-L., Pimont, F., 2012. Using periodic line fires to gain a new perspective on multi-dimensional aspects of forward fire spread. Agric. For. Meteorol. 157, 60–76.
Linn, R., Reisner, J., Colman, J.J., Winterkamp, J., 2002. Studying wildfire behavior using FIRETEC. Int. J. Wildland Fire 11 (4), 233–246.
Linn, R.R., 1997. A Transport Model for Prediction of Wildfire Behavior. Los Alamos National Lab., NM (United States).
Linn, R.R., Cunningham, P., 2005. Numerical simulations of grass fires using a coupled atmosphere–fire model: basic fire behavior and dependence on wind speed. J. Geophys. Res.: Atmospheres 110 (D13).
Linn, R.R., Sieg, C.H., Hoffman, C.M., Winterkamp, J.L., McMillin, J.D., 2013. Modeling wind fields and fire propagation following bark beetle outbreaks in spatially-heterogeneous pinyon-juniper woodland fuel complexes. Agric. For. Meteorol. 173, 139–153.
Loudermilk, E.L., Achtemeier, G.L., O'Brien, J.J., Hiers, J.K., Hornsby, B.S., 2014. High-resolution observations of combustion in heterogeneous surface fuels. Int. J. Wildland Fire 23 (7), 1016–1026. https://doi.org/10.1071/WF13160, 11pp.
Mandel, J., Beezley, J.D., Kochanski, A.K., 2011. Coupled Atmosphere-Wildland Fire Modeling with WRF-Fire Version 3.3 Supplement: A Convergence Study of the Level Set Method.
Mell, W., Jenkins, M.A., Gould, J., Cheney, P., 2007. A physics-based approach to modelling grassland fires. Int. J. Wildland Fire 16 (1), 1–22.
Mell, W., Maranghides, A., McDermott, R., Manzello, S.L., 2009. Numerical simulation and experiments of burning douglas fir trees. Combust. Flame 156 (10), 2023–2041.
Mell, W., Simeoni, A., Morvan, D., Hiers, J.K., Skowronski, N., Hadden, R.M., 2018. Clarifying the meaning of mantras in wildland fire behaviour modelling: reply to Cruz et al.(2017). Int. J. Wildland Fire 27 (11), 770–775.
Melvin, M., 2015. 2015 National Prescribed Fire Use Survey Report, Technical Report 02-15 Coalition of Prescribed Fire Councils. Inc.
Morvan, D., Meradji, S., Accary, G., 2007. Wildfire behavior study in a Mediterranean pine stand using a physically based model. Combust. Sci. Technol. 180 (2), 230–248.
Mueller, E., Mell, W., Simeoni, A., 2014. Large eddy simulation of forest canopy flow for wildland fire modeling. Can. J. For. Res. 44, 1534–1544.
Nelson, M.A., Williams, M.D., Zajic, D., Brown, M.J., Pardyjak, E.R., 2009. Evaluation of an Urban Vegetative Canopy Scheme and Impact on Plume Dispersion. Los Alamos National Lab.(LANL), Los Alamos, NM (United States).
Nelson, R.M., Butler, B.W., Weise, D.R., 2012. Entrainment regimes and flame characteristics of wildland fires. Int. J. Wildland Fire 21 (2), 127–140.
O'Brien, J., Hiers, J., Varner, J., Hoffman, C., Dickinson, M., Michaletz, S., Loudermilk, E., Butler, B., 2018. Advances in mechanistic approaches to quantifying biophysical fire effects. Curr. For. Rep. 4 (4), 161–177.
Ottmar, R.D., Hiers, J.K., Butler, B.W., Clements, C.B., Dickinson, M.B., Hudak, A.T., O'Brien, J.J., Potter, B.E., Rowell, E.M., Strand, T.M., Zajkowski, T.J., 2016. Measurements, datasets and preliminary results from the RxCADRE project – 2008, 2011 and 2012. Int. J. Wildland Fire 25 (1), 1–9.
Pardyjak, E.R., Brown, M., 2003. QUIC-URB V. 1.1: Theory and User's Guide. Los Alamos National Laboratory, Los Alamos, NM.
Parsons, R.A., Mell, W.E., McCauley, P., 2011. Linking 3D spatial models of fuels and fire: effects of spatial heterogeneity on fire behavior. Ecol. Model. 222 (3), 679–691.
Pimont, F., Dupuy, J.-L., Linn, R.R., Dupont, S., 2011. Impacts of tree canopy structure on wind flows and fire propagation simulated with FIRETEC. Ann. For. Sci. 68 (3), 523.
Rothermel, R.C., 1972. A Mathematical Model for Predicting Fire Spread in Wildland Fuels. USDA Forest Service: Intermountain Forest and Range Experiment Station, Odgen, UT.
Shaw, R.H., Seginer, I., 1987. Calculation of velocity skewness in real and artificial plant canopies. Bound.-Layer Meteor. 39, 315–332.
Singh, B., Hansen, B.S., Brown, M.J., Pardyjak, E.R., 2008. Evaluation of the QUIC-URB fast response urban wind model for a cubical building array and wide building street canyon. Environ. Fluid Mech. 8 (4), 281–312.
Sullivan, A.L., 2009a. Wildland surface fire spread modelling, 1990–2007. 1: physical and quasi-physical models. Int. J. Wildland Fire 18 (4), 349–368.
Sullivan, A.L., 2009b. Wildland surface fire spread modelling, 1990–2007. 2: empirical and quasi-empirical models. Int. J. Wildland Fire 18 (4), 369–386.
Sutton, O., 1953. Micrometeorology. McGraw-Hill, New York.
Tymstra, C., Bryce, R., Wotton, B., Taylor, S., Armitage, O., 2010. Development and Structure of Prometheus: the Canadian Wildland Fire Growth Simulation Model. Natural Resources Canada, Canadian Forest Service, Northern Forestry Centre, Edmonton, AB). Information Report NOR-X-417.
Wade, D.D., Lunsford, J.D., Dixon, M.J., Mobley, H.E., 1989. A Guide for Prescribed Fire in Southern Forests. USDA Forest Service, Atlanta, GA, p. 56.
Yedinak, K., Strand, E., Hiers, J., Varner, J., 2018. Embracing complexity to advance the science of wildland fire behavior. Fire 1 (2), 20.